Elucidating deformation pathways and interface characteristic of self-accommodated dual γ/ε phase microstructure in Fe–Mn–Si–Al alloy

Digvijay Singh[a], Alok Singh[a], Takahiro Sawaguchi[a*]

[a]Research Center for Structural Materials, National Institute for Materials Science, 1-2-1 Sengen, Tsukuba 305-0047, Japan

Digvijay Singh
singh.digvijay@nims.go.jp

Alok Singh
alok.singh@nims.go.jp

Takahiro Sawaguchi
sawaguchi.takahiro@nims.go.jp

[*] Corresponding author:

Takahiro Sawaguchi
sawaguchi.takahiro@nims.go.jp
National Institute for Materials Science,
1-2-1 Sengen, Tsukuba, Ibaraki 305-0047, Japan
Phone: +81-29-859-2416, Fax: +81-29-859-2401

Abstract

There has been an intense scientific interest in investigating the phenomenon of deformation-induced ε-ε martensite (hcp) interaction owing to the thermodynamically paradoxical reverse transformation and mechanical twinning. In this study, detailed transmission electron microscopy has been employed to examine the crystallographic orientation relationship, phase stability and boundaries between the intersection phases on the ε-ε intersections in a 10% tensile deformed Fe–30Mn–4Si–2Al alloy. The transformation/twinning scheme is systematically summarized initiating from the austenite matrix (γ) and two deformation-induced ε-martensite variants. It involves diverse intersection reactions: mechanical ε-twins, a 90º-rotating γ-phase from the γ matrix, and 90º-rotate ε-phase re-transformed from the intersection γ. All these phases share a common $<101>_{\gamma} \parallel <2\bar{1}\bar{1}0>_{\varepsilon}$ axis that is equivalent to the intersection axis of the crossing $\{111\}<1\bar{2}1>_{\gamma}$ shears and interrelated with rotational angles with respect to the axis. The boundaries between the intersection γ and neighboring ε-phase are inclined from the corresponding $\{111\}_{\gamma}\|\{10\bar{1}1\}\varepsilon$ planes. By means of the phenomenological theory of martensite crystallography (PTMC), the inclination of the boundary is rationalized by considering the lattice-invariant shear on the double $\{111\}_{\gamma}$ plane inside the intersection γ to satisfy the invariant plane condition of the boundary.

Keywords: Martensite transformation, Twinning, TRIP steels, Transmission electron microscopy (TEM), ε-martensite

1. Introduction

Fe-Mn-Si-based alloys are well known for their shape memory effect, owing to their unique reversible phase transformation characteristics which occur when exposed to a specific stimulus, such as temperature or stress [1]. The phase transformation involves a deformation induced transformation of γ-austenite (fcc) to hexagonal close packed (hcp) ε-martensite, which is recoverable upon heating [2]. The shape memory effect in Fe-Mn-Si-based alloys is of significant importance due to its potential applications in various fields, including aerospace, medical, and automotive industries [3–5]. Additionally, their high damping capacity and excellent corrosion resistance make them attractive for use in structural and damping applications, for example fish plate couplings of rails of industrial cranes [6] and seismic dampers [7].

Deformation induced martensitic transformation and mechanical twinning is of immense interest in various austenitic alloys, including austenitic stainless steel, medium Mn-, and high-Mn steel, owing to the transformation induced plasticity (TRIP) and twinning induced plasticity (TWIP) phenomenon which results in outstanding synergy between strength and ductility observed in these materials [8–10]. The stacking fault energy (SFE), deformation level (strain/strain rate), and crystal orientations of the parent phase are the key factors that governs the deformation mechanisms in various austenitic alloys [11–15]. Depending upon the SFE and thermodynamic phase stability, several modes of martensitic transformation have been established, namely direct transformation ($\gamma \rightarrow \varepsilon/\acute{\alpha}$) or two-step transformation ($\gamma \rightarrow \varepsilon \rightarrow \acute{\alpha}$) [16–19]. Sawaguchi et al. developed a low SFE based Fe-15Mn-10Cr-8Ni-4Si damping alloy [20], which shows excellent low-cycle fatigue properties with the aid of bi-directional transformation induced plasticity (B-TRIP) or reversible $\gamma \rightleftharpoons \varepsilon$ martensitic transformation [21]. Besides

SFE criteria, crystallographic orientation relationship plays an important role in martensitic transformation. The fcc to hcp transformation ($\gamma \rightarrow \varepsilon$) is achieved through the orderly $\{111\}\langle 1\bar{2}1\rangle_{\gamma}$ Shockley partial shear movement within alternative {111} close pack planes of γ-lattice. Based upon Schmidt criteria, several ε-variants with different habit planes may operate simultaneously under critical stress invariant in the parent γ-matrix. Due to the orderly-tetrahedral geometry of $\{111\}\gamma$ cubic planes, multiple variants of ε-martensite with different habit planes intersect each other, which results in the change of atomic arrangements within the intersection volume [22–24]. Hence, at a particular temperature and with a specific chemical composition in an alloy, multiple intersection products can coexist, and their presence is determined by the crystallographic orientation. Zhang et al. observed that the ε-intersection reaction is significantly driven by the orientation of the intersecting shears, which can be classified into two types: Type I with crossing shears perpendicular to the intersection axis and Type II with crossing shears inclined at an angle of 30 degrees [22]. Moreover, the ε-ε intersection volume has been identified as a potential nucleation site for α-martensite (bcc) phase in metastable austenitic steels [25]. Alongside α-martensite, several other intersection products, including 90° reverted austenite and ε-martensite phases (γ_{90}, ε_{90}), γ-twins, and ε-twins $(10\bar{1}2, 10\bar{1}1)$ have been observed at ε-ε intersection volume in Fe-Mn-Si-based damping alloys [2,22–26].

The ε-ε intersection structures in γ matrix are highly significant concerning the material performance, including shape memory effects, strain hardening, and fatigue properties [2,7,20,21,27–31]. The ε-ε intersection structures act as a source, barrier, or sink of dislocations during deformation by generating new interfaces with the adjacent phases. An initial study utilizing transmission electron microscopy (TEM) was conducted

by Yang and Wayman [23,24]. They engaged in comprehensive discussions and speculations concerning potential structures. Interestingly, some of the structures initially identified as 'secondary variants' were later revealed to be twins of the ε-phase, as demonstrated by Matsumoto et al. [26]. Zhang et al. conducted an electron backscatter diffraction study to investigate the orientation dependence of ε-martensite in polycrystalline high-Mn steels, with a specific focus on the intersection of ε plates [22]. After a 10% tensile deformation, microstructural observation strongly showed orientation dependent structures, primarily attributed to the Schmid factor. Grain orientations near <414> exhibited only a single variant of ε martensite, whereas a very few ε plates were observed in grains oriented along <001>, which is an orientation for easy slip. In addition, a new γ-phase with 90º orientation from the parent γ phase was discovered at Type-I intersection along <001> ─ <101> [23–25] . Furthermore, $\{10\bar{1}2\}$ ε-twin were identified at Type II intersections along <001> ─ <111>. Furthermore, the twinning mechanism of the ε-martensite in the Fe–30Mn–6Si shape memory alloy was thoroughly explored by Zhang and Sawaguchi [32]. Their findings revealed the existence of $\{10\bar{1}2\}$ and $\{10\bar{1}1\}$ type twinning in specimens deformed at room temperature, corresponding to Type I and Type II intersection, respectively. Although there have been detailed studies by EBSD and some by dark field TEM, the crystallographic and interface orientations were not clearly brought out. The crystallographic orientation relationships and interface configuration of these ε-ε intersection structures are crucial for understanding the microstructure evolution, underlying accommodation mechanism, and the mechanical properties exhibited by these materials. The martensitic transformation and twinning processes are strongly influenced by the crystallographic orientation of the parent phase, and the resulting microstructure is highly dependent on the crystallographic orientation

relationship and interface configuration of the ε-martensite and parent γ-regions. Therefore, a detailed understanding of these phenomena is essential for tailoring the mechanical properties of Fe-Mn-Si-based alloys and optimizing their performance in various applications.

Although we have primarily demonstrated ε-ε intersections using EBSD, it's important to note that EBSD has resolution limitations, which hinder a clear resolution of the intricate microstructures at the interface. To address these challenges, here we present a detailed TEM study that provides a clear view of interfaces and traces of plane within the ε-martensite plates. The observations are explained by modifying the phenomenological theory of martensite crystallography (PTMC) and possible sequence of transformations.

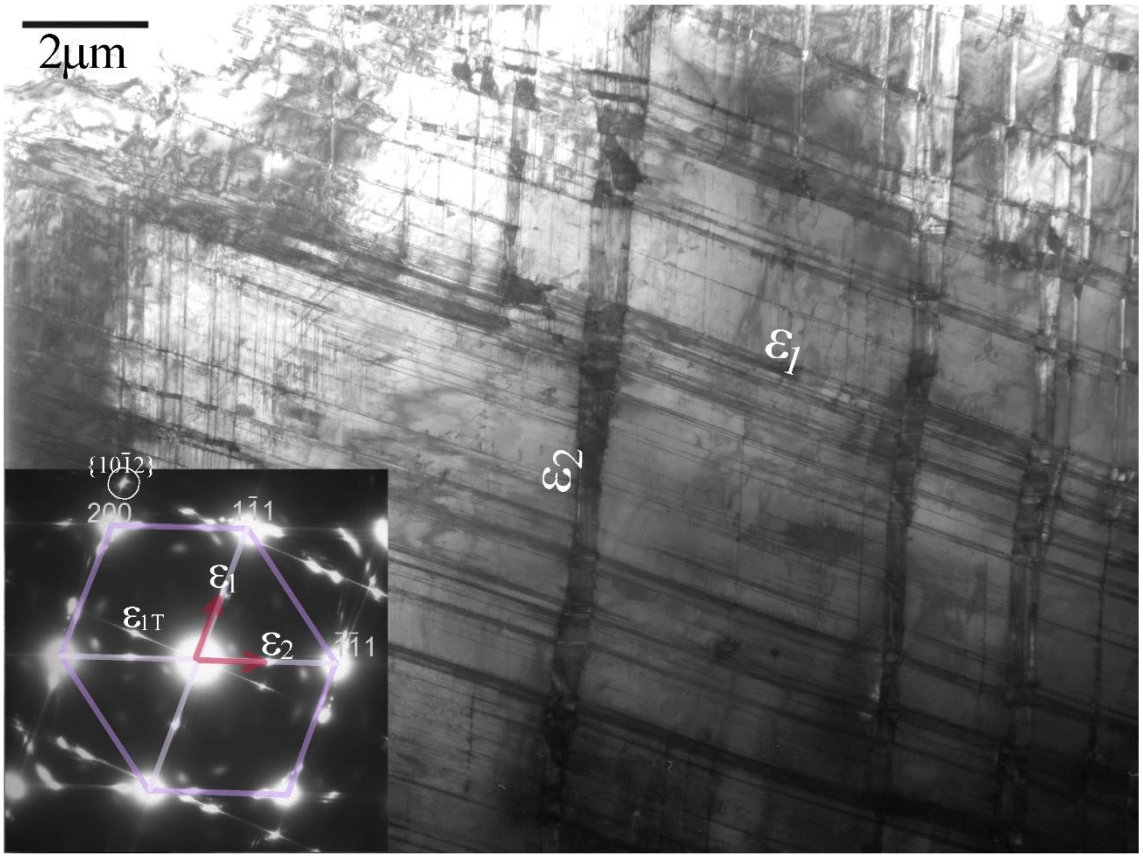

Figure 1: *Epsilon martensite plates viewed in a grain oriented along a <110> zone axis. Two variants of martensitic plates ε_1 and ε_2 are observed along traces of two {111} planes*

indexed as ($1\bar{1}1$*) and (*$\bar{1}\bar{1}1$*).*

2. Experimental

A polycrystalline Fe-30Mn-4Si-2Al (mass %) alloy was prepared by induction melting. The resulting alloy was hot forged and hot rolled at 1000 ºC, and then subjected to water quenching. Subsequently, it was subjected to a solution treatment at 1000 ºC. The specimen was plastically deformed to 10% strain in tension, with the deformation direction being along the rolling direction. The deformed samples were thinned by mechanical grinding and then using jet polishing for observation and analysis using transmission electron microscopy (TEM) on a JEOL 2000FX microscope.

3. Results

A bright field micrograph along <110> zone axis of matrix γ phase in Fig. 1 shows plates along two directions, labeled ε_1 and ε_2. The inset diffraction pattern shows that these two sets of plates occur on two variants of {111} parent γ phase. A diffraction spot at 1/2 {111} corresponds to (0001) reciprocal vector of the ε phase. Thus, taking lattice parameter of the γ phase to be 3.61 Å, $c_\varepsilon \sim 4.17$ Å. Two intersections of two sets of plates ε_1 and ε_2 are shown in Fig. 2. The structure of these two intersections will be examined in detail in the following.

One of the two intersection of two variants of ε plates in Fig. 2 is shown in Fig. 3. The crystallographic relationship of the matrix γ with each variant of ε plates is shown in the diffraction patterns. The γ-ε phases follow Shoji-Nishiyama (S-N) orientation relationship. From these diffraction patterns, the a_ε parameter of ε is determined to be 2.55 Å. In the bright field image, the ε plates are along {111} plane traces of parent γ phase, designated γ_1. Inside the ε plates parallel lines are observed, which are presumed to be stacking faults formed during transformation. Inside the intersection region of the

plates, γ phase was found, designated γ_2, as will be described here. In this γ_2 region, two sets of parallel lines are observed, which are traces of faults on {111} planes of this phase. Traces of these planes show that the orientation of γ_2 is 90º rotated about <110> axis of γ_1.

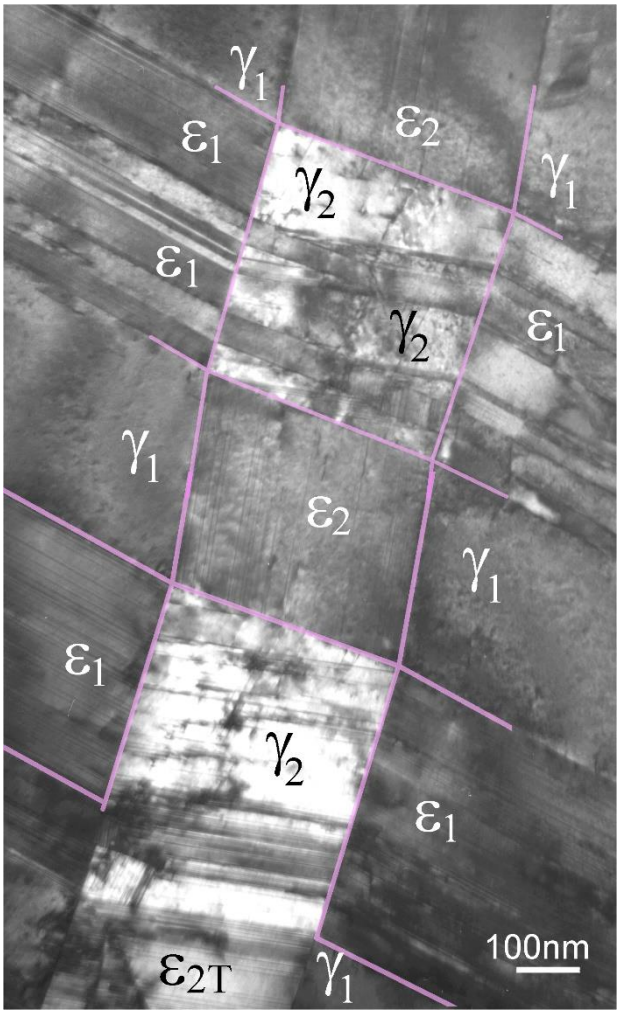

Figure 2: *A bright field micrograph showing details of two intersection sites of ε plates ε_1 and ε_2 in a grain oriented along a <110> zone axis. ε-γ interfaces are outlined.*

Twinning is an important deformation mode in hexagonal phases, commonly of $\{10\bar{1}2\}$ type. Twinning was observed inside the ε plates. Fig. 4 shows twins in a plate of ε_1 variant. Twin boundaries are pointed out by open arrows. The inset diffraction pattern shows that these twins are of the type $\{10\bar{1}2\}$. A coincident $\{10\bar{1}2\}$spot is marked in the

figure. The twin boundaries in the bright field micrograph are observed to be roughly on $\{10\bar{1}2\}$ planes.

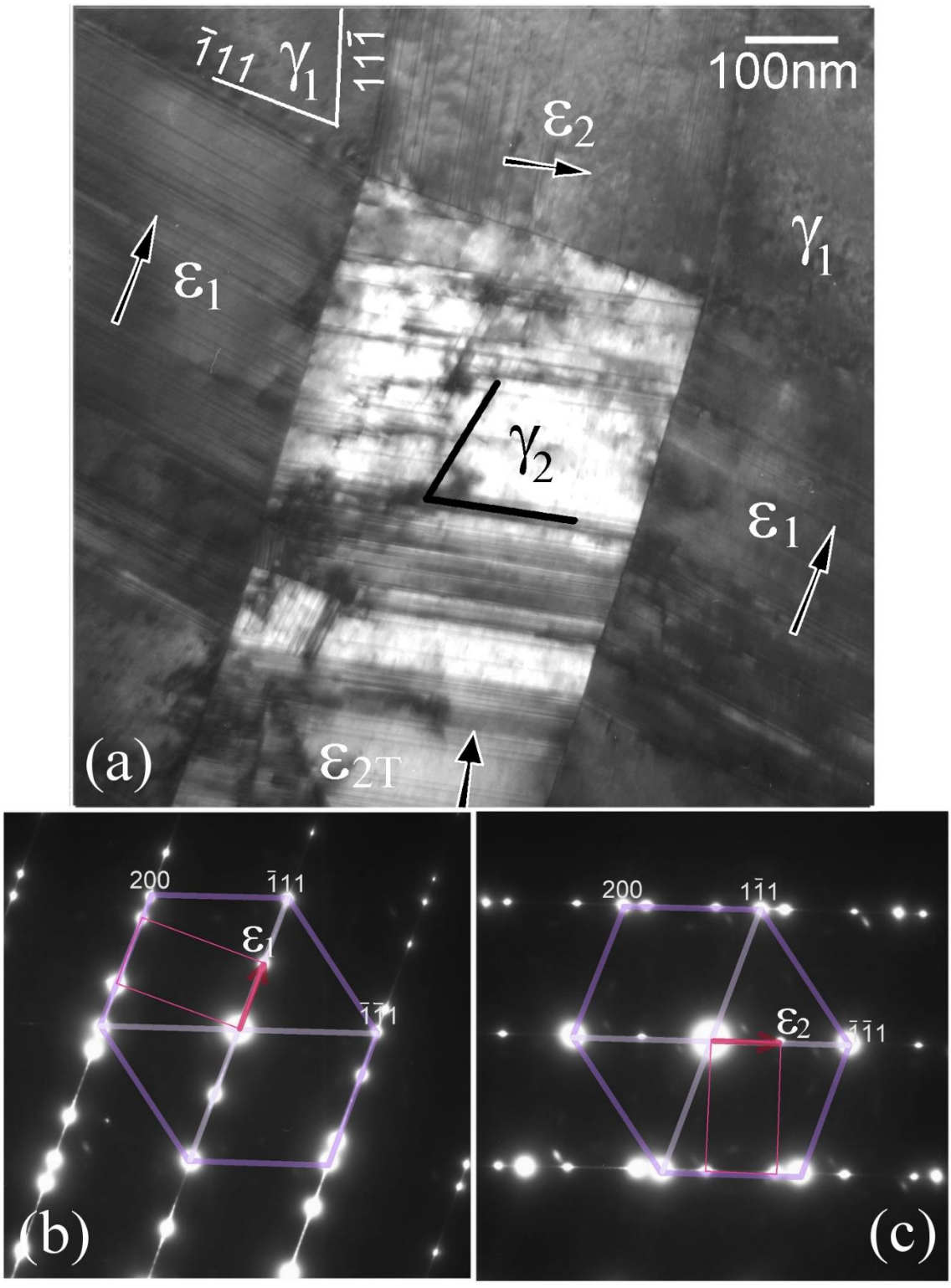

Figure 3: *(a) A bright field micrograph showing one of the intersections shown in Fig. 2. Two variants of martensite plates ε_1 and ε_2 are along planes $(1\bar{1}1)$ and $(\bar{1}\bar{1}1)$, respectively, of matrix γ_1. The orientation and the crystallographic relationship of the martensite plates with respect to the matrix are shown in the composite diffraction patterns in (b) and (c), for the two variants ε_1 and ε_2. c-axes of ε phase are marked by arrows. At the intersection of the plates in (a) occurs another variant of the FCC matrix, γ_2.*

The intersection of ε plates could be complex, consisting of twins of ε and variant γ_2 of the matrix phase γ_1. Fig. 5 shows a complete sequence of transformations. At the top of the scheme is a matrix γ unit cell oriented along a <110> axis. A shear along either of the {111} planes results in hexagonal unit cell in orientation ε_1 or ε_2. A twinning on one of the two $\{10\bar{1}2\}$planes (parallel to this orientation) in each of ε_1 and ε_2 produces a twin, in orientations described as positive or negative. This type of twins is reported to form at the ε variant intersections [26]. Note that the ε have near S-N orientation relationship, but not precisely; their basal planes are nearly parallel to either of {111} planes of the γ_2, but deviate by approximately 4º. Formation of twins in the negative sense are unfavorable under shear I+II reaction. Twins of ε_1 and ε_2 are oriented differently from each other. In a third possibility, a shear on the prismatic plane of ε can transform it again to γ phase. This γ phase (γ_2) is oriented 90º with respect to the parent γ phase. Whether transforming from ε_1 or ε_2, the orientation of the γ_2 remains the same. Thus, it can form at the intersections of ε_1 and ε_2. The γ_2 was theoretically predicted by Sleeswyk [33], and experimentally determined by EBSD [22,25]. Yang and Wayman proposed that the γ_2 immediately re-transformed into ε, designated as $\varepsilon_{90}(1)$ and $\varepsilon_{90}(2)$ [23,24]. The ε_{90} has the exact S-N orientation relationship with γ_2.

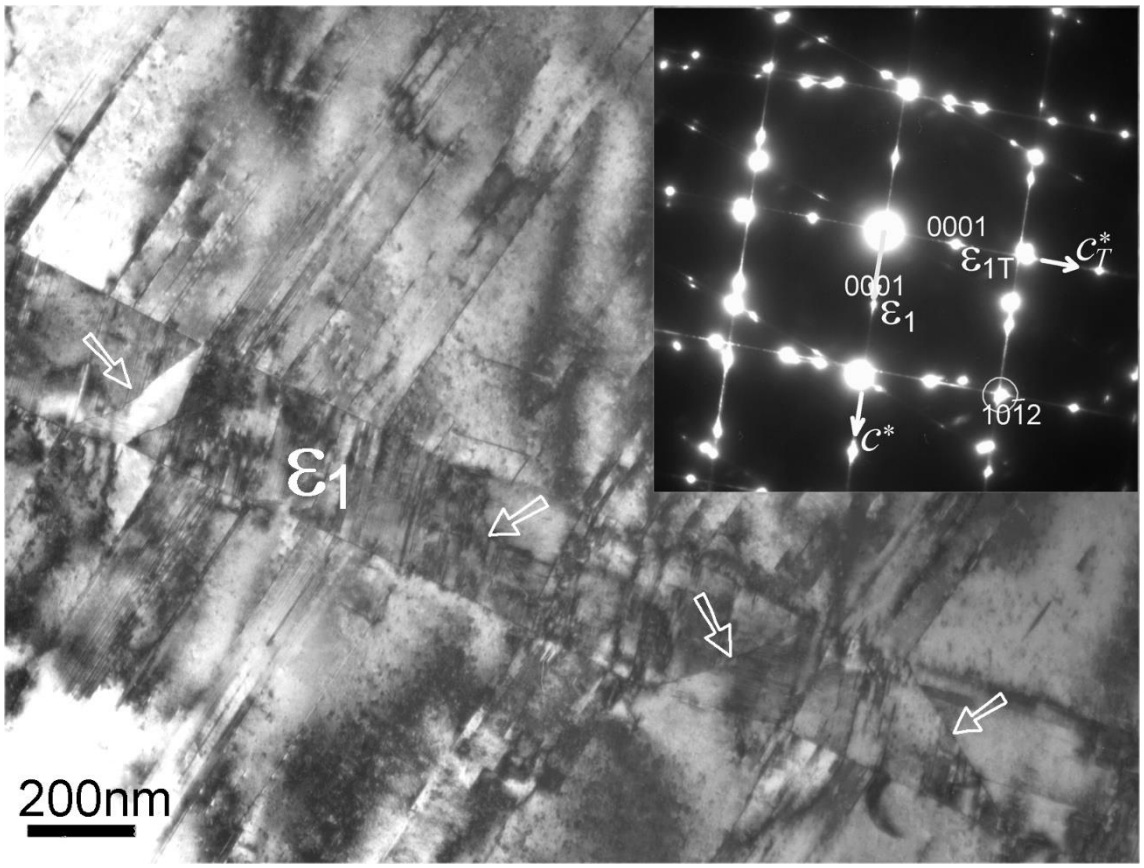

Figure 4: *A bright field micrograph showing twins in a martensite plate ε_1. The twin boundaries are marked with arrows. The inset diffraction pattern from one of the twins shows that the twin boundaries are on a $\{10\bar{1}2\}$ plane common to the ε_1 matrix and its twin.*

Another example is taken from Fig. 2 and shown in detail along with diffraction patterns in Fig. 6. A thick plate of ε_2 runs nearly vertically through the center of the micrograph in Fig. 6(a). The thickness and number of ε_1 plates running on either side of intersection with ε_2 plate are not uniform. In the diffraction patterns of Fig. 6(b) and (c), $(0001)_\varepsilon$ spots corresponding to ε_1 and ε_2 are observed. In addition, one more (0001) spot occurs, which corresponds to the twin of ε_2 (marked ε_{2T}), as predicted by schematic in Fig. 5. The crystallographic orientation of γ_1 is marked by a hexagon in the diffraction pattern of Fig. 6(b). Plates of ε_1 and ε_2 follow the S-N orientation relationship with γ_1. In Fig. 6(c) the orientation of γ_2 is marked by a similar hexagon (diffraction spots of γ_2 are very

prominent in this diffraction pattern). It is clearly observed that the twin of ε_2, ε_{2T}, forms S-N orientation relationship with γ_2.

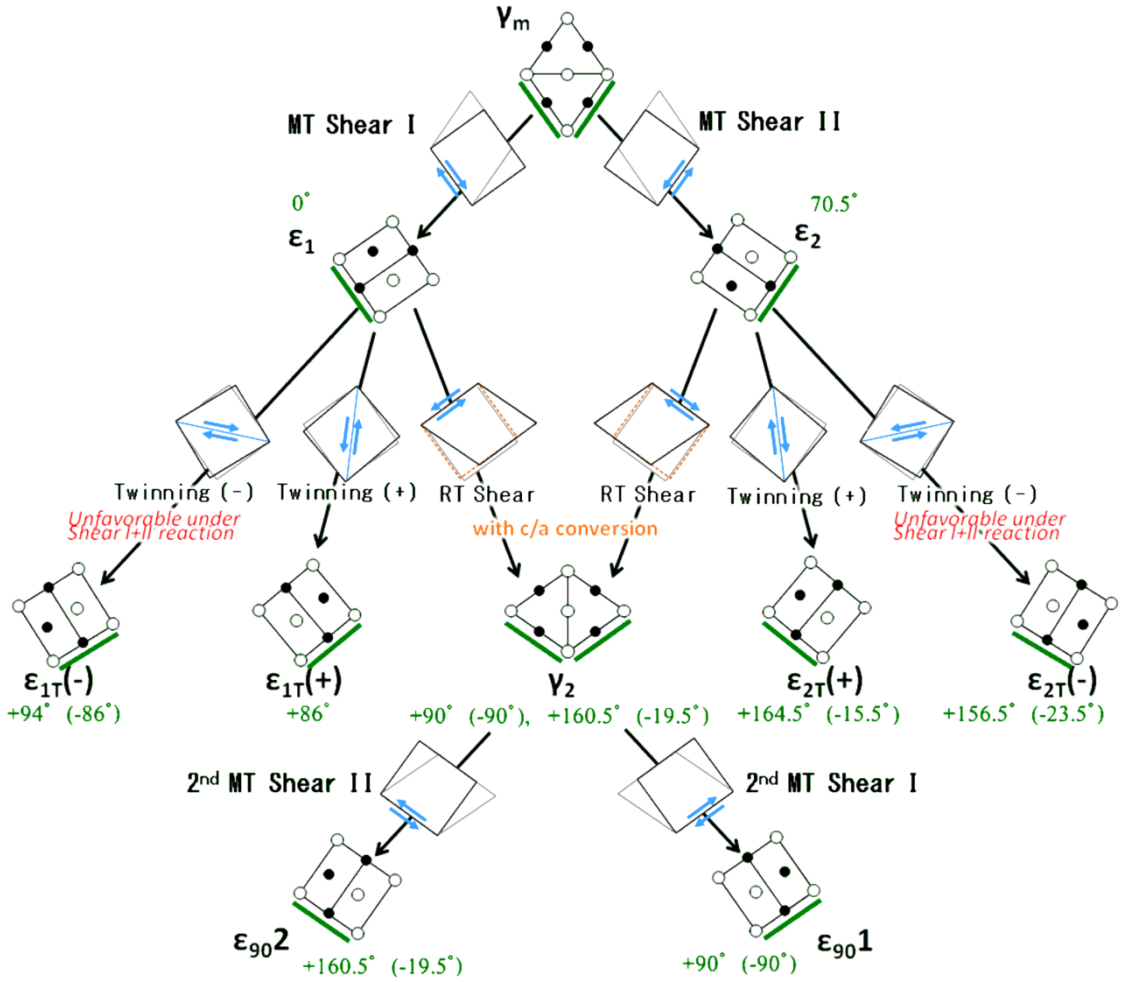

Figure 5: *A scheme of transformations from the parent phase γ_m (or γ_1, shown at the top). MT shear along orientations I or II lead to transformation to ε phases ε_1 or ε_2. Twinning shears lead to twins ε_{1T} or ε_{2T}, while an RT shear transforms an ε phase to another variant γ_2 of the parent γ phase. A further MT shear on the γ_2 phase leads to 90° variants of ε phase. The orientations of crystals are represented by rotation angles (clockwise: positive) of $\{111\}_\gamma$ or $\{0001\}_\varepsilon$ planes with respect to $\{111\}_{\gamma m}$.*

γ_2 phase occurs in the upper part of the intersection of ε_1 and ε_2 plates in Fig. 6(a). Below this, a segment of ε_2 plate appears again, but which is twinned in to ε_{2T} on the right side. Immediately below occurs γ_2 phase. Thus there occurs a sandwich of ε_{2T}

between γ_2 phase, which maintain the S-N orientation relationship between them. It can be roughly seen that the interface between these phases is on $\{111\}_{\gamma 2}$ and $(0001)_{\varepsilon 2T}$. In the lower part of the micrograph, ε_{2T} occurs at the intersection of ε_1 and ε_2. This ε_2 twin is sandwiched between two slabs of ε_2, but the interface is clearly not on $\{10\bar{1}2\}$ planes. Occurrence of γ_2 at the intersection of plates can be clearly made out in Fig. 3(a) by the visible faults on its $\{111\}$ planes. Below the intersection, the plate orientation is ε_{2T}, instead of ε_2. It makes a matching interface with γ_2 on $\{111\}_{\gamma 2} \parallel (0001)_{\varepsilon 2T}$ planes.

Plate configuration in a wider area are shown in Fig. 7. A ε_2 plate runs vertically through the middle of the micrograph, and is twinned in to a band of ε_{2T} in the lower part. The diffraction patterns in Fig. 7(b) shows the orientation of γ_1, (c) shows diffraction pattern of ε_{2T} twin, (d) shows the orientation relationship of γ_1 with ε_1 and ε_2, and (e) shows the orientation of the γ_2 phase and its orientation relationship with ε_{2T}. In Fig. 7(a), γ_1 located at the bottom right establishes interfaces with ε_1 and ε_2, as seen in the diffraction pattern of Fig. 7(d). The γ_2 phase at the intersection of ε_1 and ε_2 plates does not make any major orientation relationship with either ε_1 or ε_2, as observed in the diffraction pattern of Fig. 7(f). However, to the left of this γ_2 phase occurs ε_{1T}, Fig. 7(g), but with no apparent interface with ε_1. To the left of it occur alternate layers of γ_2 and ε_{1T}. A diffraction between these two is shown in Fig. 7(h) and (i). Both (h) and (i) show the same diffraction pattern, but (h) highlights the crystallographic relationship of γ_1 to ε_2 while (i) highlights the relationship of γ_2 to ε_{1T} by drawing hexagons to show the orientations of γ_1 or γ_2.

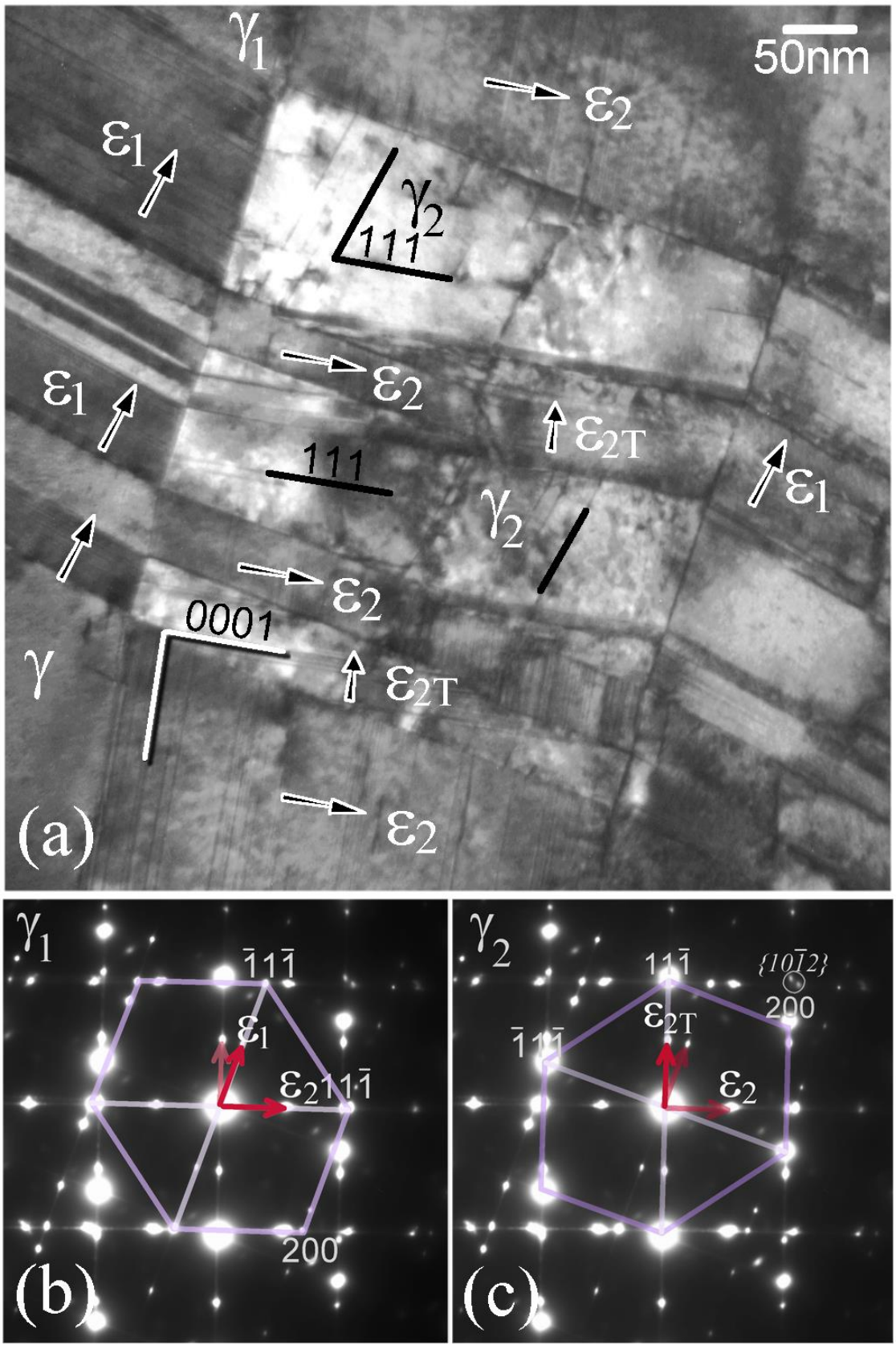
γ1
50nm
ε2
ε1
γ2
111
ε2
ε1
ε2T
111
ε1
γ2
ε2
0001
γ
ε2T
ε2
(a)
γ1
1̄11̄
ε1
ε2
11̄
200
(b)
γ2
11̄
{10̄12}
200
ε2T
1̄11̄
ε2
(c)

Figure 6: *(a) A complex intersection of ε_1 and ε_2 plates showing twins ε_{2T} of ε_2 and reoriented matrix γ_2, as marked on the micrograph. (b) and (c) show the same diffraction pattern from the whole region. Diffraction from matrix γ_1 is marked in (b) while that from γ_2 is marked in (c), showing their crystallographic relationships with martensite plates and their twins. In the bright field micrograph of (a), c-axes of ε phase are marked by arrows and traces of {111} planes of γ_2 are marked by lines.*

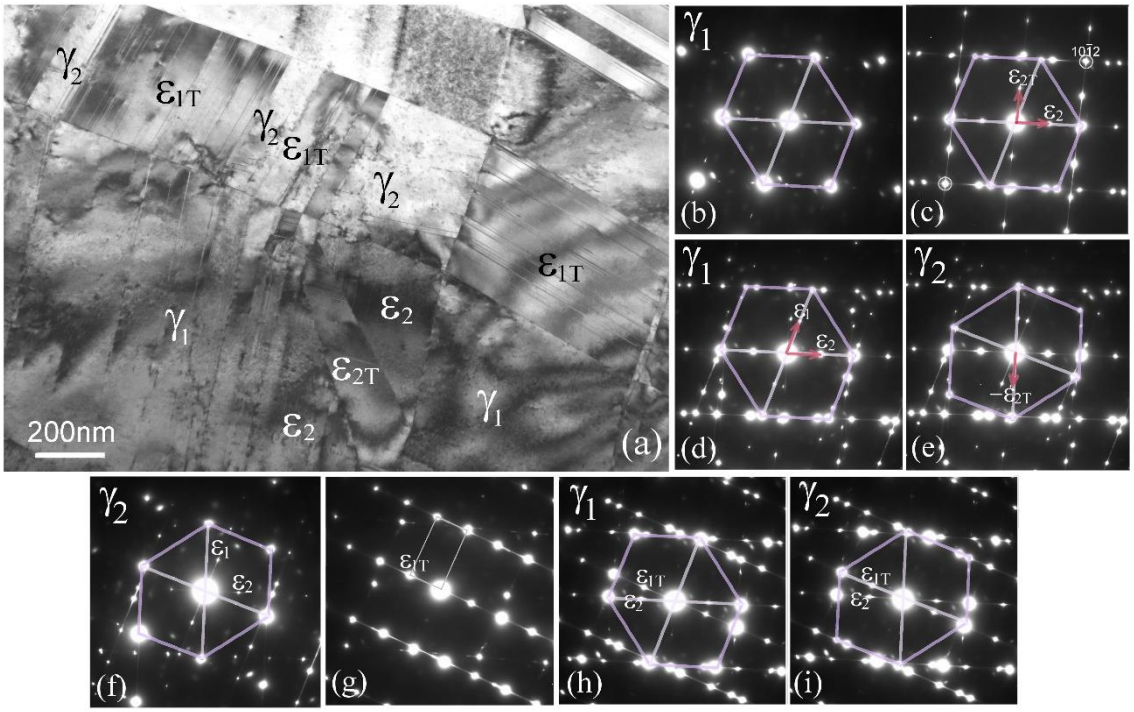

Figure 7: *(a) Epsilon martensite plates and their twins viewed in a grain oriented along a <111> zone axis. (b) A diffraction pattern from the matrix γ_1. (c) Diffraction from plate ε_2 and its twin ε_{2T} observed at bottom center of the micrograph in (a) (matrix γ_1 spots are also present). (d, e) A composite diffraction pattern from the matrix γ_1, plates ε_1 and ε_2, and twin ε_{2T}, as well as γ_2. γ_2 is observed at the intersection of plates ε_1 and ε_2 in (a). Diffraction spots of γ_1 and its relationship to ε_1 and ε_2 are marked in (d), while γ_2 and its relationship to epsilon phase twin ε_{2T} is marked in (e). (f) A diffraction pattern from γ_2 (diffraction spots from ε_1 and ε_2 are also observed). (g) Diffraction pattern from a region related to ε_1 by twinning, ε_{1T}, observed in the upper left of the micrograph in (a). (h, i) A composite diffraction pattern from matrix γ_1, ε_2, ε_{1T} and γ_2 observed in the upper center region of the micrograph in (a). γ_1 and its relationship to ε_2 is marked in (h), while γ_2 and its relationship to ε_{1T} is marked in (i).*

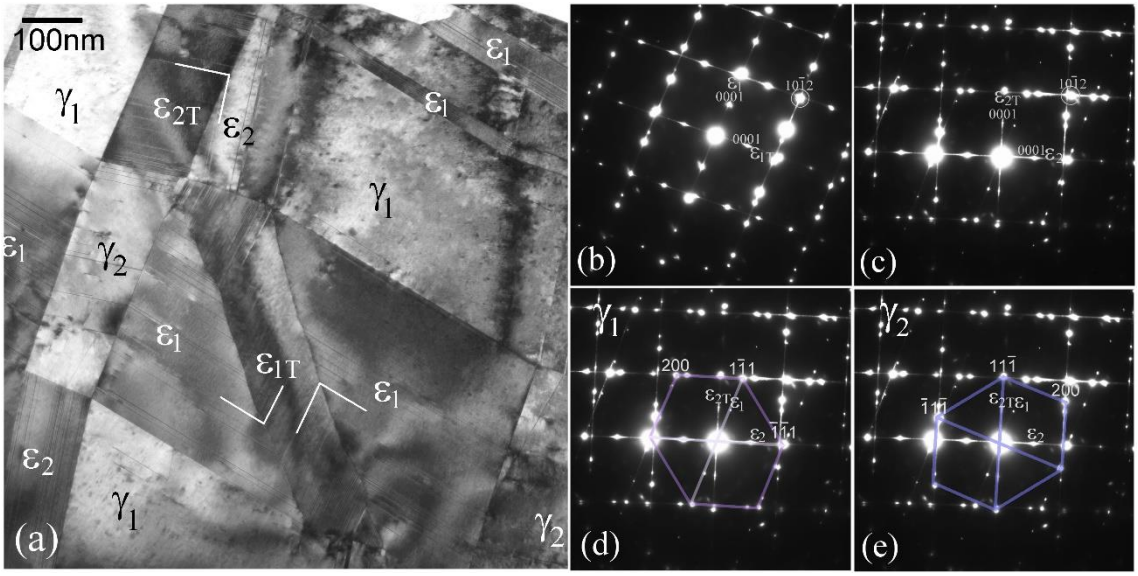

Figure 8: *(a) A bright field micrograph showing interaction of martensite plates and their twins. A band of twin occurs in ε_1 plate. A segment of ε_2 plate is its own twin ε_{2T}, next to which grows a ε_2 plate. A diffraction pattern in (b) confirms the ε_1 twin and (c) shows the ε_2 twin. The latter diffraction pattern shows ε_1, ε_2 and ε_{2T} with respect to (d) γ_1 and (e) γ_2.*

Fig. 8 shows interaction of ε_1 and ε_2 plates and their twins. At left center in Fig. 8(a) is γ_2 phase at an intersection of ε_1 and ε_2 plates. The upper neighbor of the γ_2 is in not ε_2, but its twin ε_{2T}. The ε_1 block dominating this micrograph shows a diagonal twin band across it, the twin boundaries being on the $\{10\bar{1}2\}$ planes. The diffraction pattern of this twin is shown in Fig. 8(b). From the geometry of the plates, the upper edge of the twinned domain ε_{1T} should make an interface with a γ_1. However, the upper part of the twin in fact makes an interface with a domain of ε_2. This ε_2 domain makes an interface with ε_{2T} on left, with which it is crystallographically twin related (Fig. 8(c)). The interface is, however, not on a twinning plane $\{10\bar{1}2\}$, but on the original interface of ε_{2T} with γ_1. It can be argued that this region of ε_2 forms to minimize the interfacial energies between ε_{1T}, γ_1 and ε_{2T} phases. γ_1 does not form matching crystallographic orientations with ε_{1T} or ε_{2T}. ε_2 forms as a buffer, with Shoji-Nishiyama orientation relationship with γ_1 and twin

relationship with ε_{2T}. The exact matching length of the interface of ε_{1T} with ε_2 indicates that the formation of ε_2 is triggered by ε_{1T}. The interface between ε_{1T} and ε_2 is nearly perpendicular (~85°) to the basal planes of ε_2 (the basal planes of ε_2 and ε_{1T} are about 18° apart). Observation at the lower end of the ε_{1T} band also indicates triggering of formation of ε_2 plates in γ_1.

4. Discussion

In martensitic transformation, orientation relationship between austenite and product martensite phases, shape strain from displacive character, and the nature of interfaces are among the important crystallographic features [34–39]. Understanding the microstructure evolution, accommodation mechanism, and mechanical properties exhibited by high-Mn steels relies heavily on the crystallographic orientation relationships and interface configuration of the ε-ε intersection structures. The crystallographic orientation of the parent phase significantly impacts both the martensitic transformation and twinning processes. As a result, the resulting microstructure is highly contingent upon the crystallographic orientation relationship and interface configuration between the ε-martensite and parent γ-regions [32,38]. Olsen and Cohen proved that the coherent interface could incorporate specific type of partial dislocation that play a crucial role in facilitating lattice deformation during the transformation between the two phases and ensuring the continuity of the lattice structure [40]. Thermodynamically there are two phases in the deformed Fe-Mn-Si-Al alloy, but two different orientations of γ phase and four orientations of ε phase, each making interfaces with neighboring phases. Thus, it appears that interfacial energies are important for the stability of the microstructure. All observations here show that all the interfaces are very sharp. Inside the phases transformed from γ_1 (ε and γ_2), planar defects parallel to the basal hexagonal plane or

{111} planes are observed, marking the orientation of these planes clearly.

Orientation relationships are plotted on stereographic projections in Fig. 9. In the S-N orientation relationship between γ and ε plates, at the interface of planes $\{111\}_\gamma$ with $\{0001\}_\varepsilon$, three equivalent prominent match of directions occur: $<110>_\gamma \parallel <11\bar{2}0>_\varepsilon$. There are three planar matches of the kind $\{110\}_\gamma \parallel \{1\bar{2}10\}_\varepsilon$. Fig. 9(b) shows the orientation relationship of γ_2 and ε plates. There is a planar match of $\{111\}_{\gamma 2} \parallel \{0110\}_\varepsilon$, in which occur a match of $<110>_\gamma \parallel <11\bar{2}0>_\varepsilon$ directions and two near matches of $<110>_{\gamma 2} \parallel <2\bar{1}\bar{1}3>_\varepsilon$. The orientation relationship between γ_2 and ε_T twin is similar to that between γ and ε. Similarly, the orientation relationship between γ and twin ε_T is the same as that between γ_2 and ε. The similarity also holds for the interfaces between the phases. In Fig. 7(a), an interface is observed between ε_{1T} and γ_1 phases in the left part of the micrograph. Inside the γ_1 phase, fine plates of ε_2 are observed, seemingly originating from the interface with ε_{1T}. Thus, there is an interface between ε_2 and ε_{1T}, whose orientation is the same as the orientation of the interface between γ_2 and ε_2 to the right of it. This interface orientation is different from the orientation of the interface between γ_1 and ε_1 phases (e.g., on the right in this micrograph). The orientation of this interface halfway between a set of {111} planes each in γ_1 (on which plates of γ_2 occur) and in γ_2 (on which plates of ε_{1T} occur). In other words, the interface intersects the angle between the basal planes in ε_{1T} and ε_2 plates.

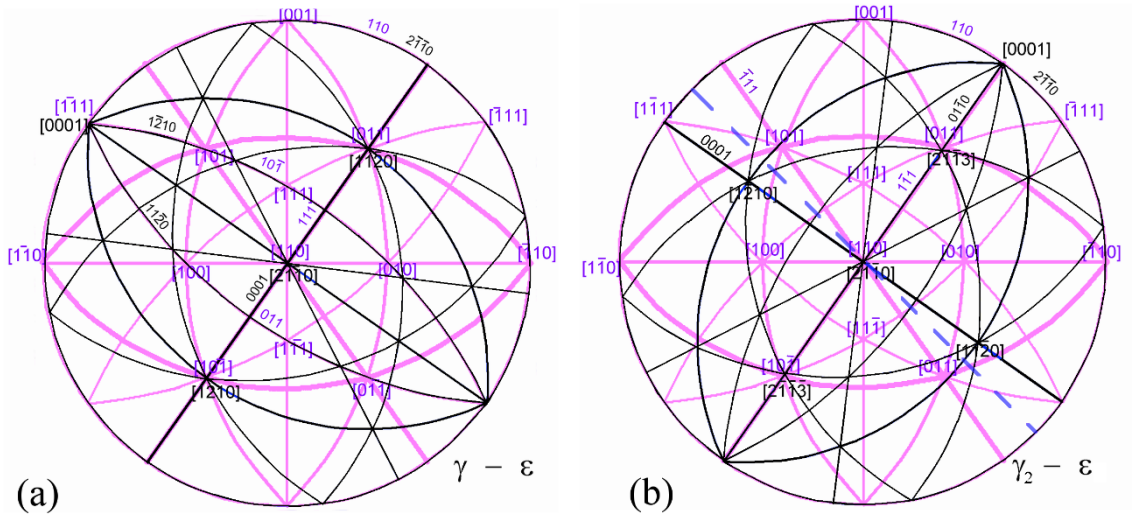

Figure 9: *Stereographic projections showing the orientation relationships between (a) γ and ε phases and (b) γ_2 and ε. The austenite phases (γ and γ_2) are depicted using colored lines, while ε phase is indicated by black lines.*

The interfaces between γ_1 and ε_1 or ε_2 are on {111} planes of γ and {0001} plane of ε phase, as would be expected from the crystallographic and transformation mechanism. Similar relationship holds between γ_2 phase and twin ε_{2T}. However, interfaces of γ_2 and ε phases at intersections are not on any major planes of either phase. This will be analyzed and discussed below. Analysis based on trace of the planes and the corresponding diffraction patterns show that these interfaces are on planes at mid orientations between $\{111\}_{\gamma 1}$ and $\{111\}_{\gamma 2}$ corresponding to the interfaces γ_1–ε and γ_2–ε, respectively. The angle between these {111} planes of γ_1 and γ_2 are about 19.5º, the mid plane roughly corresponding to {755} of either phase. A $\{03\bar{3}1\}$ plane of ε makes interface with the {755} plane of γ_2. The position of the interface plane is shown by a dashed line in the stereogram of Fig. 9(b), bisecting $\{\bar{1}11\}_{\gamma 2}$ and $(0001)_{\varepsilon}$ planes.

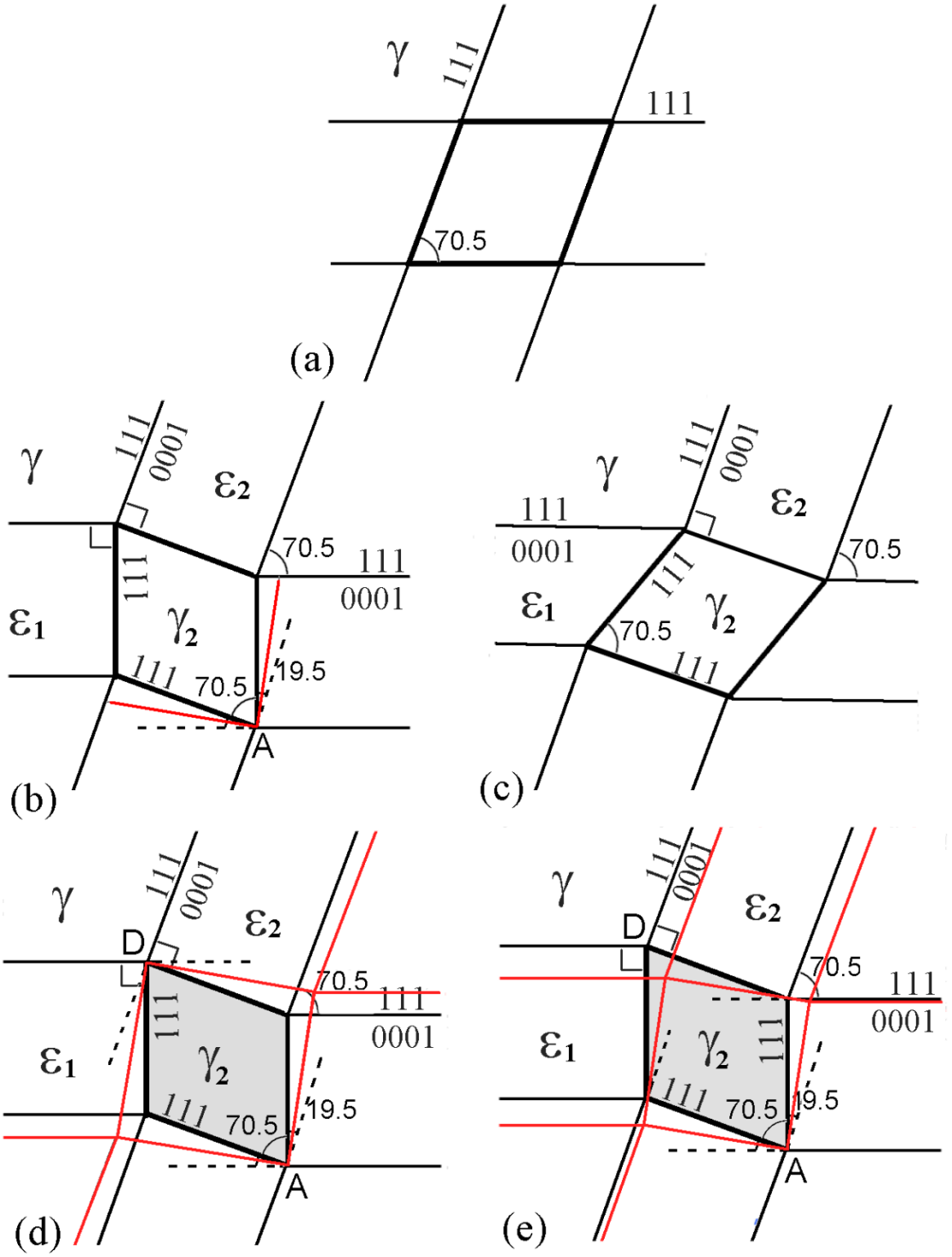

Figure 10: *Possible mechanism of formation of interfaces at intersections. (a) Orientation of two sets of {111} planes in γ matrix, observed along a <110> axis. (b) An intersection of ε plates with the γ matrix in the same orientation. The intersection region γ_2 is rotated with respect to the matrix γ by 90º. (c) Similar configuration as in (b), but in which intersection region γ_2 is rotated with respect to the matrix by 19.5º (after* [23]*). (d,*

e) Derived from (b), two different configurations of interfaces between γ_2 region and ε plates are shown. In both cases the interfaces are intersections of the matrix γ {111} plane and the γ_2 {111} plane.

Possible ε intersection configurations are considered by Yang and Wayman [23]. Following this, Fig. 10(a) shows two sets of {111} planes of matrix γ phase viewed along a <110> axis. Yang and Wayman considered two possibilities of rotation of intersection region γ_2 with respect to the matrix. In one, γ_2 is rotated with respect to the matrix by 90º, and in another by 19.5º (90º - 70.5º, in positive or negative directions), as shown in Fig. 10(b) and (c), respectively. In the former case (Fig. 10(b)), all interfaces are perpendicular to γ_{111} planes, i.e., on the basal (0001) planes of ε plates. As has been seen in this study, this orientation relationship holds, but the actual interface orientations are not as drawn. From point marked A in this figure, two lines are drawn along intersections of the angle between the γ_2 rhombus and traces of matrix {111} planes (dashed lines), shown as red lines. These two lines are close to the actual position of the interfaces. While in this diagram the intersection rhombus becomes a square or a rectangle, the experimentally observed rhombuses are defined by angles of 96º and 84º, as outlined in Fig. 2. Using this construction, two possible constructions of interfaces can be made. As shown in Fig. 10(d), this construction is made symmetrically to the opposite edge marked D. As a result, the area of γ_2 is increased, and both plates ε_1 and ε_2 are thickened. In construction shown in Fig. 10(e), the other two edges are drawn inside of the γ_2 rhombus. In this way, the area of γ_2 and the thicknesses of plates ε_1 and ε_2 are nearly preserved. However, it requires that one segment of each of ε_1 and ε_2 shift sideways (as plates ε_1 on the left and ε_2 on top in Fig. 10(e).

The intersection shown in Fig. 6(a) has a very complex structure. This must be

because the thickness and position of ε_1 plates are not matched on either side of the intersection with ε_2. However, the whole complex intersection is within a rhombus with a geometry as constructed in Fig. 10. This raises a possibility that ε_1 plates formed after the formation of ε_2 plates. γ_2 forms in the upper parts of the intersection of ε_1 and ε_2. At the bottom part of the intersection, ε_{2T} occurs. It forms wide interfaces with ε_2 on two sides (with which it has twin relationship, but does not form interfaces on twin plane), with only a small segment with ε_1.

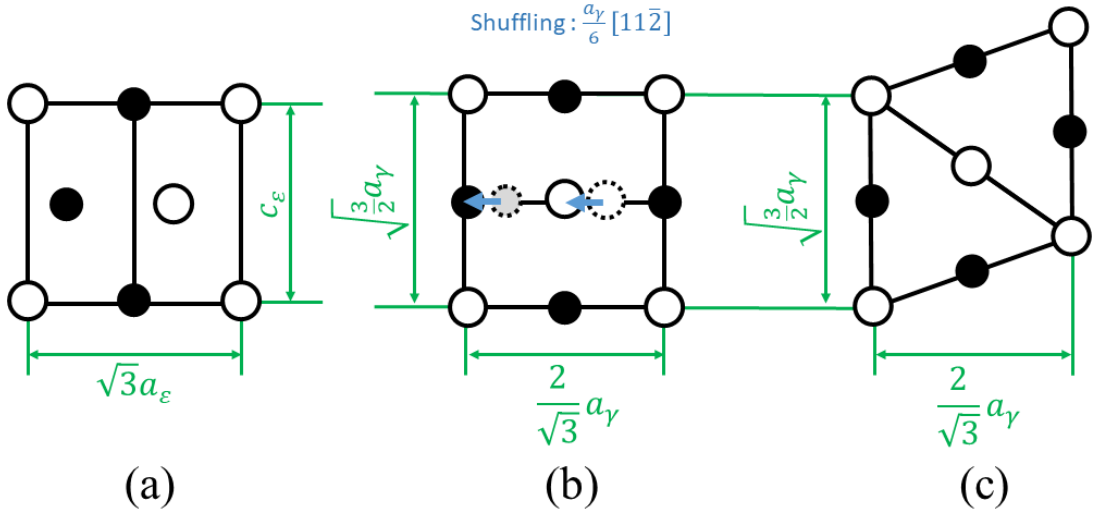

Figure 11: *The process of the ε to γ reverse transformation at ε − ε intersection.*

4.1. Scheme of transformations

Thus, the orientation relationships between the intersection γ phase, ε_1 and ε_2 agree well with the Yang and Wayman (Y−M) model [23,24], but the observed boundaries between them are significantly inclined from the corresponding crystallographic planes of $\{1010\}_\varepsilon \| \{111\}_\gamma$. In this section, the reason for the inclination of the boundaries is discussed by means of the phenomenological theory of martensite crystallography (PTMC), which was developed for studying the crystallography for the γ to α' martensitic

transformation [41–44].

The first requirement in PTMC is that an austenite/martensite boundary should be an invariant plane in which all lines are neither distorted nor rotated [44]. In the γ to α' martensitic transformation the lattice distortion proposed by Bain (Bain distortion) is widely accepted, which is consisting of a contraction along one $<001>_{\gamma}$ axis and uniform expansions along the other two $<001>_{\gamma}$ axes [45]. In the Bain distortion there is no invariant plane, and therefore a complementary shear and rotation are needed to obtain it. The second requirement of PTMC is that the complementary shear must be a lattice-invariant shear with which no change in crystal structure occurs. With using matrix calculation, the shape deformation $P_{\gamma\to\alpha}$ can be expressed as the product of the Bain distortion $B_{\gamma\to\alpha}$, lattice-invariant shear $S_{\gamma\to\alpha}$, and rotation $R_{\gamma\to\alpha}$ as follows [46–48].

$$P_{\gamma\to\alpha} = R_{\gamma\to\alpha}\, S_{\gamma\to\alpha}\, B\gamma_{\to\alpha} \quad (1)$$

On the other hand, in the case of the γ to ε martensitic transformation, the lattice distortion is a simple shear displacement on the $\{111\}_{\gamma}\|\{0001\}_{\varepsilon}$ plane. If we neglect the small shrinkage of lattice volume during the transformation, the $\{111\}_{\gamma}\|\{0001\}_{\varepsilon}$ plane is invariant, and neither complementary shear nor rotation is needed to complete the shape deformation. The shape deformation $P_{\gamma\to\varepsilon}$ is equivalent with the homogeneous shear $B_{\gamma\to\varepsilon}$, $P_{\gamma\to\varepsilon} = B_{\gamma\to\varepsilon}$. As a consequence, the γ /ε boundary is parallel to the $\{111\}_{\gamma}\|\{0001\}_{\varepsilon}$ plane, and the crystallographic orientation relationship (S–N relationship: $\{111\}_{\gamma}\|\{0001\}_{\varepsilon}$, $<101>_{\gamma} \| <11\bar{2}0>_{\varepsilon}$) is directly obtained with respect to the simple shear process.

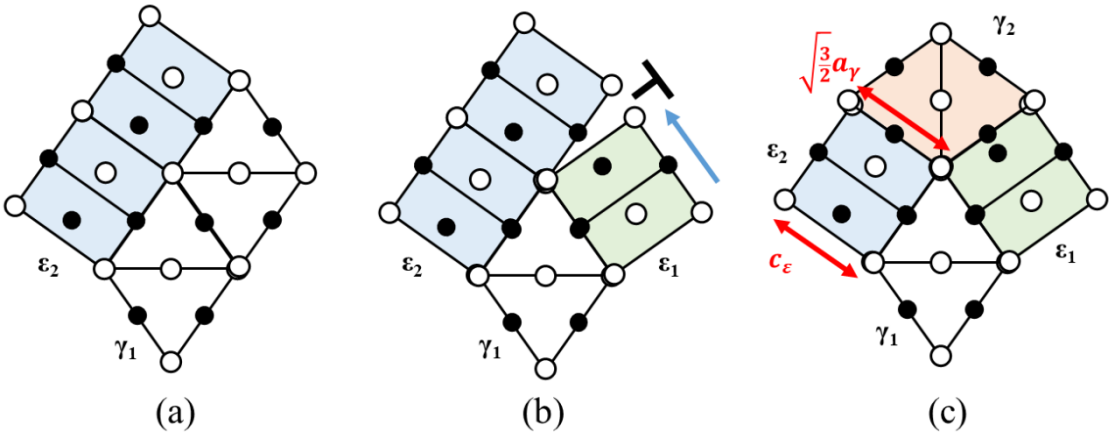

Figure 12: *The lattice correspondence between the phases. (a) S-N orientation relationship between γ_1 and γ_2, (b) approaching ε_1, (c) lattice mismatch between the intersection γ_1 with ε_1 and ε_2.*

However, in the ε to γ reverse martensitic transformation at the ε – ε intersection, a significantly large lattice distortion must also be taken into the account. As schematically drawn in Fig. 11, the transformation from ε to the intersection γ is made by two steps: (1) the + 6.96 % expansion along [0001] (c_ε to $\sqrt{3}/2a_\gamma$) and - 5.68 % contraction along $[10\bar{1}0]$ ($\sqrt{3}a_\varepsilon$ to $2/\sqrt{3}\ a_\gamma$) accompanying atomic shuffling ((a) to (b)), and (2) reverse transformation shear ((b) to (c)). The distortion causes a lattice mismatch between the intersection γ with ε_1 and ε_2, as shown in Fig. 12. The ε_2 has S–N orientation relationship with the parent γ phase (a) and encounters the $a_\gamma/6\ \{111\}\langle 1\bar{2}1\rangle_\gamma$ transformation shear (b) from the ε_1 growing upward to the left. The intersection γ_2 produced by the crossing transformation shear (c) has expanded surface which are incoherent with the neighboring ε phases. The $\{111\}_\gamma \| \{0001\}_\varepsilon$ planes therefore do not satisfy the invariant plane condition, and the complementary lattice-invariant shear should be considered to find an invariant boundary plane.

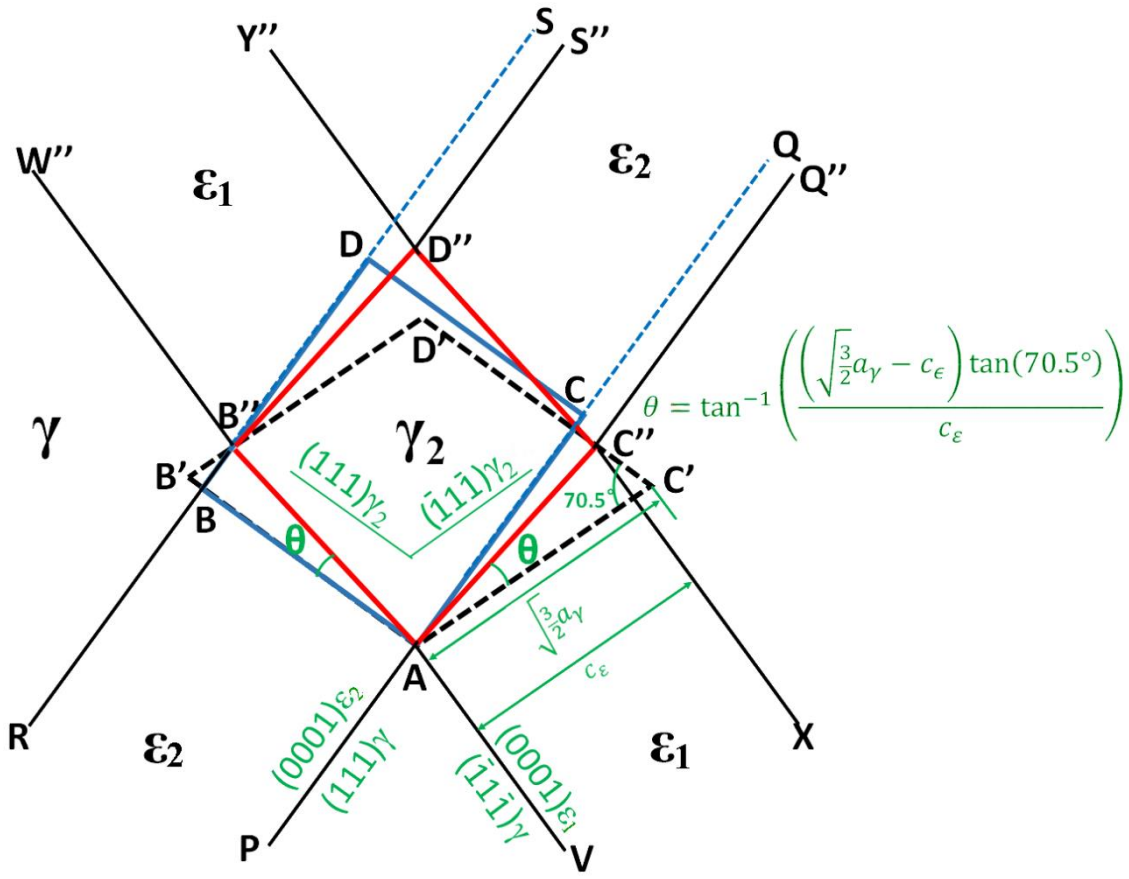

Figure 13: *A plausible mechanism for reverse transformation at ε - ε intersection.*

The invariant boundary plane can be determined by finding two nonparallel invariant lines. One of such invariant lines is evidently the $[10\bar{1}]_\gamma \parallel [2\bar{1}\bar{1}0]\varepsilon$ axis (here we neglect the slight extension of the line of + 0.0419 %), while another invariant line can be determined by considering the geometry on the plane normal to the axis, as shown in Fig. 13. In this figure, we assume that the most plausible lattice-invariant shear is dislocation glide on two $\{111\}_\gamma$ planes inside γ_2. To maintain the continuity of the matter, basal slip inside the ε phases should also be activated. The area ABDC in ε_2 should be distorted into AB'D'C' by the lattice distortion and then into AB" D" C" by the subsequent lattice-invariant shear. The point C" must stay at the intersection of C'D' and XC, since C" is associated with C' by the lattice invariant shear on $(111)_\gamma$ plane and with

C by the lattice-invariant shear on $(0001)_\varepsilon$ plane. From this geometry, the angle θ in the figure is calculated as 5.04º. The same argument is applicable to the interface between the incident ε_2 and γ_2.

The shape deformation at the ε–ε intersection $P_{\varepsilon\rightarrow\gamma int}$ can be expressed as the product of the lattice distortion described in Fig. 11 $B_{\varepsilon\rightarrow\gamma int}$, and the lattice-invariant shear on double $\{111\}_\gamma$ plane $S_{\varepsilon\rightarrow\gamma int}$, as follows.

$$P_{\varepsilon\rightarrow\gamma int} = S_{\varepsilon\rightarrow\gamma int}\, B_{\varepsilon\rightarrow\gamma int} \qquad (2)$$

Without additional rotation, the lattice obtained through this calculation satisfy the experimentally observed orientation of the γ_2 phase with the parent γ_1, ε_1, and ε_2.

5. Conclusions

The detailed TEM investigation on the ε-ε martensite interaction in 10 % tensile deformed Fe-30Mn-4Si-2Al (mass %) austenitic alloy led to the following conclusions:

1. At the intersections of the ε plates, a variant γ_2 of γ phase is formed, which is oriented with respect to the original matrix γ_1 by a rotation of 90º about a <110> axis nearly perpendicular to the plane of deformation. At these intersections, the interface between ε plates and γ_2 are not on major planes of ε prismatic and $\{111\}_{\gamma 2}$, but on a plane intersecting these two planes.
2. During deformation, the hexagonal ε plates twin by $\{10\bar{1}2\}$ type of twinning (which rotates the c-axis by about 86º). These twins make the same orientation relationship, Shoji-Nishiyama orientation relationship, with γ_2 phase as between ε and γ phases, with the interface being on $\{111\}_{\gamma 2}$ and $\{10\bar{1}1\}_{\varepsilon T}$ prismatic planes. The overall interfacial energy is thus lowered on formation of ε twins. Various

interfaces formed at plate-plate, plate-twin and twin-twin interactions are established clearly.

3. The phases γ_1, ε_1 and its twin ε_{1T}, along with their orientational variants γ_2, ε_2 and ε_{2T} make several configurations of interfaces. The ε_2 (or ε_1) plate adjacent to the intersection γ_2 may twin (forming a ε_2-ε_{2T} (or ε_1-ε_{1T}) twin interface), such that a γ_2-ε_2 (or γ_2-ε_1) interface is replaced with a γ_2-ε_{2T} (or γ_2 -ε_{1T}) interface.
4. A scheme of shear deformations has been applied to show that on application of simultaneous shear on two adjacent {111} planes of the parent γ_1 phase, two different variants ε_1 and ε_2 of ε can be formed. Application of shear on prismatic planes of these two variants can result in a γ phase of same variant, γ_2.
5. A detailed model of such a transformation has been constructed to show the geometrical transformation of the interfaces.

Acknowledgments

The authors express their gratitude to Prof. Kaneaki Tsuzaki for encouragement to carry out this work and for valuable discussions. A part of this work was supported by a Grant-in-Aid for Early-Career Scientists (21H01659) from the Japan Society for the Promotion of Science (JSPS), Japan.

Reference:

[1] H. Li, D. Dunne, N. Kennon, Factors influencing shape memory effect and phase transformation behaviour of Fe–Mn–Si based shape memory alloys, Materials Science and Engineering: A. 273–275 (1999) 517–523. https://doi.org/10.1016/S0921-5093(99)00391-3.

[2] A. Sato, E. Chishima, K. Soma, T. Mori, Shape memory effect in $\gamma \rightleftarrows \epsilon$ transformation in Fe-30Mn-1Si alloy single crystals, Acta Metallurgica. 30 (1982) 1177–1183. https://doi.org/10.1016/0001-6160(82)90011-6.

[3] E. Ghafoori, E. Hosseini, C. Leinenbach, J. Michels, M. Motavalli, Fatigue behavior of a Fe-Mn-Si shape memory alloy used for prestressed strengthening, Mater Des. 133 (2017) 349–362. https://doi.org/10.1016/J.MATDES.2017.07.055.

[4] T. Sawaguchi, T. Maruyama, H. Otsuka, A. Kushibe, Y. Inoue, K. Tsuzaki, Design Concept and Applications of FeMnSi-Based Alloys ®from Shape-Memory to Seismic Response Control, (2016). https://doi.org/10.2320/matertrans.MB201510.

[5] R. Drevet, Y. Zhukova, P. Malikova, S. Dubinskiy, A. Korotitskiy, Y. Pustov, S. Prokoshkin, Martensitic Transformations and Mechanical and Corrosion Properties of Fe-Mn-Si Alloys for Biodegradable Medical Implants, Metall Mater Trans A Phys Metall Mater Sci. 49 (2018) 1006–1013. https://doi.org/10.1007/S11661-017-4458-2/TABLES/2.

[6] T. Maruyama, T. Kurita, S. Kozaki, K. Andou, S. Farjami, H. Kubo, Materials Science and Technology Innovation in producing crane rail fishplate using Fe-Mn-Si-Cr based shape memory alloy Innovation in producing crane rail fishplate using Fe-Mn-Si-Cr based shape memory alloy, (2013). https://doi.org/10.1179/174328408X302585.

[7] T. Sawaguchi, P. Sahu, T. Kikuchi, K. Ogawa, S. Kajiwara, A. Kushibe, M. Higashino, T. Ogawa, Vibration mitigation by the reversible fcc/hcp martensitic transformation during cyclic tension–compression loading of an Fe–Mn–Si-based shape memory alloy, Scr Mater. 54 (2006) 1885–1890. https://doi.org/10.1016/J.SCRIPTAMAT.2006.02.013.

[8] S. Martin, S. Wolf, U. Martin, L. Kru¨ger, K. Kru¨ger, D. Rafaja, Deformation Mechanisms in Austenitic TRIP/TWIP Steel as a Function of Temperature, Metallurgical and Materials Transactions A. (n.d.). https://doi.org/10.1007/s11661-014-2684-4.

[9] G. Frommeyer, U. Brüx, P. Neumann, Supra-Ductile and High-Strength Manganese-TRIP/TWIP Steels for High Energy Absorption Purposes, ISIJ

International. 43 (2003) 438–446. https://doi.org/10.2355/ISIJINTERNATIONAL.43.438.

[10] O. Grässel, L. Krüger, G. Frommeyer, L.W. Meyer, High strength Fe–Mn–(Al, Si) TRIP/TWIP steels development — properties — application, Int J Plast. 16 (2000) 1391–1409. https://doi.org/10.1016/S0749-6419(00)00015-2.

[11] A.Y. Chen, H.H. Ruan, J. Wang, H.L. Chan, Q. Wang, Q. Li, J. Lu, The influence of strain rate on the microstructure transition of 304 stainless steel, Acta Mater. 59 (2011) 3697–3709. https://doi.org/10.1016/J.ACTAMAT.2011.03.005.

[12] J.X. Zou, K.M. Zhang, T. Grosdidier, C. Dong, Y. Qin, S.Z. Hao, D.Z. Yang, Orientation-dependent deformation on 316L stainless steel induced by high-current pulsed electron beam irradiation, Materials Science and Engineering: A. 483–484 (2008) 302–305. https://doi.org/10.1016/J.MSEA.2006.07.179.

[13] I. V. Kireeva, Y.I. Chumlyakov, The orientation dependence of γ-α′ martensitic transformation in austenitic stainless steel single crystals with low stacking fault energy, Materials Science and Engineering: A. 481–482 (2008) 737–741. https://doi.org/10.1016/J.MSEA.2006.12.204.

[14] I. Karaman, H. Sehitoglu, Y.I. Chumlyakov, H.J. Maier, The deformation of low-stacking-fault-energy austenitic steels, JOM. 54 (2002) 31–37. https://doi.org/10.1007/BF02700983/METRICS.

[15] D.T. Pierce, J.A. Jiménez, J. Bentley, D. Raabe, J.E. Wittig, The influence of stacking fault energy on the microstructural and strain-hardening evolution of Fe–Mn–Al–Si steels during tensile deformation, Acta Mater. 100 (2015) 178–190. https://doi.org/10.1016/J.ACTAMAT.2015.08.030.

[16] S. Li, P.J. Withers, S. Kabra, K. Yan, The behaviour and deformation mechanisms for 316L stainless steel deformed at cryogenic temperatures, (2023). https://doi.org/10.1016/j.msea.2023.145279.

[17] S. Curtze, V.T. Kuokkala, Dependence of tensile deformation behavior of TWIP steels on stacking fault energy, temperature and strain rate, Acta Mater. 58 (2010) 5129–5141. https://doi.org/10.1016/J.ACTAMAT.2010.05.049.

[18] Y.K. Lee, C.S. Choi, Driving force for γ → ε martensitic transformation and stacking fault energy of γ in Fe-Mn binary system, Metall Mater Trans A Phys Metall Mater Sci. 31 (2000) 355–360. https://doi.org/10.1007/S11661-000-0271-3/METRICS.

[19] S. Allain, J.P. Chateau, O. Bouaziz, S. Migot, N. Guelton, Correlations between the calculated stacking fault energy and the plasticity mechanisms in Fe–Mn–C alloys, Materials Science and Engineering: A. 387–389 (2004) 158–162.

https://doi.org/10.1016/J.MSEA.2004.01.059.

[20] T. Sawaguchi, I. Nikulin, K. Ogawa, K. Sekido, S. Takamori, T. Maruyama, Y. Chiba, A. Kushibe, Y. Inoue, K. Tsuzaki, Designing Fe–Mn–Si alloys with improved low-cycle fatigue lives, Scr Mater. 99 (2015) 49–52. https://doi.org/10.1016/J.SCRIPTAMAT.2014.11.024.

[21] F. Yoshinaka, T. Sawaguchi, S. Takamori, S. Emura, Transformation-induced plasticity via γ → ε → α' and γ → ε → γ martensitic transformations in Fe–15Mn–10Cr–8Ni–4Si alloy, Materials Science and Engineering: A. 833 (2022) 142583. https://doi.org/10.1016/J.MSEA.2021.142583.

[22] X. Zhang, T. Sawaguchi, K. Ogawa, F. Yin, X. Zhao, Orientation dependence of variant selection and intersection reactions of ϵ martensite in a high-manganese austenitic steel, Http://Dx.Doi.Org/10.1080/09500839.2011.596492. 91 (2011) 563–571. https://doi.org/10.1080/09500839.2011.596492.

[23] J.H. Yang, C.M. Wayman, On secondary variants formed at intersections of ϵ martensite variants, Acta Metallurgica et Materialia. 40 (1992) 2011–2023. https://doi.org/10.1016/0956-7151(92)90187-J.

[24] J.H. Yang, C.M. Wayman, Intersecting-shear mechanisms for the formation of secondary ϵ martensite variants, Acta Metallurgica et Materialia. 40 (1992) 2025–2031. https://doi.org/10.1016/0956-7151(92)90188-K.

[25] X. Zhang, T. Sawaguchi, K. Ogawa, F. Yin, X. Zhao, A structure created by intersecting ϵ martensite variant plates in a high-manganese steel, Http://Dx.Doi.Org/10.1080/14786435.2011.608734. 91 (2011) 4410–4426. https://doi.org/10.1080/14786435.2011.608734.

[26] S. Matsumoto, A. Sato, T. Mori, Formation of h.c.p. and f.c.c. twins in an Fe□Mn□Cr□Si□Ni alloy, Acta Metallurgica et Materialia. 42 (1994) 1207–1213. https://doi.org/10.1016/0956-7151(94)90137-6.

[27] T. Sawaguchi, L.G. Bujoreanu, T. Kikuchi, K. Ogawa, M. Koyama, M. Murakami, Mechanism of reversible transformation-induced plasticity of Fe–Mn–Si shape memory alloys, Scr Mater. 59 (2008) 826–829. https://doi.org/10.1016/J.SCRIPTAMAT.2008.06.030.

[28] A. Sato, E. Chishima, Y. Yamaji, T. Mori, Orientation and composition dependencies of shape memory effect IN Fe-Mn-Si alloys, Acta Metallurgica. 32 (1984) 539–547. https://doi.org/10.1016/0001-6160(84)90065-8.

[29] F.X. Yin, H. Xia, J.H. Feng, M.H. Cai, X. Zhang, G.K. Wang, T. Sawaguchi, Mechanical properties of an Fe-30Mn-4Si-2Al alloy after rolling at different temperatures ranging from 298 to 1073 K, Materials Science and Engineering: A.

725 (2018) 127–137. https://doi.org/10.1016/J.MSEA.2018.03.079.

[30] I. Nikulin, T. Sawaguchi, A. Kushibe, Y. Inoue, H. Otsuka, K. Tsuzaki, Effect of strain amplitude on the low-cycle fatigue behavior of a new Fe–15Mn–10Cr–8Ni–4Si seismic damping alloy, Int J Fatigue. 88 (2016) 132–141. https://doi.org/10.1016/J.IJFATIGUE.2016.03.021.

[31] I. Nikulin, N. Nagashima, F. Yoshinaka, T. Sawaguchi, Superior fatigue life of Fe-15Mn-10Cr-8Ni-4Si seismic damping alloy subjected to extremely high strain amplitudes, Mater Lett. 230 (2018) 257–260. https://doi.org/10.1016/J.MATLET.2018.07.123.

[32] X. Zhang, T. Sawaguchi, Twinning of deformation-induced ε-martensite in Fe-30Mn-6Si shape memory alloy, Acta Mater. 143 (2018) 237–247. https://doi.org/10.1016/J.ACTAMAT.2017.10.009.

[33] A.W. Sleeswyk, Note on the F.C.C.→H.C.P. and H.C.P.→F.C.C. transformations, Https://Doi.Org/10.1080/14786436208213294. 7 (2006) 1597–1601. https://doi.org/10.1080/14786436208213294.

[34] P.M. Kelly, Martensite crystallography—The role of the shape strain, Materials Science and Engineering: A. 438–440 (2006) 43–47. https://doi.org/10.1016/J.MSEA.2006.02.065.

[35] J.K. Mackenzie, J.S. Bowles, The crystallography of martensite transformations II, Acta Metallurgica. 2 (1954) 138–147. https://doi.org/10.1016/0001-6160(54)90103-0.

[36] J.S. Bowles, J.K. Mackenzie, The crystallography of martensite transformations III. Face-centred cubic to body-centred tetragonal transformations, Acta Met., 1954, Vol. 2. 138 (1954) 224–224. https://doi.org/10.1016/0001-6160(54)90163-7.

[37] B.P.J. Sandvik, C.M. Wayman, CHARACTERISTICS OF LATH MARTENSITE: PART I. CRYSTALLOGRAPHIC AND SUBSTRUCTURAL FEATURES., Metallurgical Transactions. A, Physical Metallurgy and Materials Science. 14 A (1983) 809–822. https://doi.org/10.1007/BF02644284/METRICS.

[38] G.B. Olson, M. Cohen, A general mechanism of martensitic nucleation: Part II. FCC → BCC and other martensitic transformations, Metallurgical Transactions A. 7 (1976) 1905–1914. https://doi.org/10.1007/BF02659823/METRICS.

[39] G.B. Olson, M. Cohen, Interphase-boundary dislocations and the concept of coherency, Acta Metallurgica. 27 (1979) 1907–1918. https://doi.org/10.1016/0001-6160(79)90081-6.

[40] G.B. Olson, M. Cohen, Interphase-boundary dislocations and the concept of coherency, Acta Metallurgica. 27(12) (1979) 1907-1918.

https://doi.org/10.1016/0001-6160(79)90081-6.

[41] R.C. Pond, S. Celotto, J.P. Hirth, A comparison of the phenomenological theory of martensitic transformations with a model based on interfacial defects, Acta Mater. 51 (2003) 5385–5398. https://doi.org/10.1016/S1359-6454(03)00395-1.

[42] A.G. Crocker, THE PHENOMENOLOGICAL THEORIES OF MARTENSITE CRYSTALLOGRAPHY, Le Journal de Physique Colloques. 43 (1982) C4-209. https://doi.org/10.1051/JPHYSCOL:1982426.

[43] W.Z. Zhang, G.C. Weatherly, A comparative study of the theory of the O-lattice and the phenomenological theory of martensite crystallography to phase transformations, Acta Mater. 46 (1998) 1837–1847. https://doi.org/10.1016/S1359-6454(97)00435-7.

[44] C.M. Wayman, The phenomenological theory of martensite crystallography: Interrelationships, Metallurgical and Materials Transactions A. 25 (1994) 1787–1795. https://doi.org/10.1007/BF02649029/METRICS.

[45] E.C. Bain, NY Dunkirk, The nature of martensite, Trans. AIME. 70(1) (1924) 25-47.

[46] J.S. Bowles, J.K. Mackenzie, The crystallography of martensite transformations I, Acta Metallurgica. 2 (1954) 129–137. https://doi.org/10.1016/0001-6160(54)90102-9.

[47] J.S. Bowles, J.K. Mackenzie, The crystallography of martensite transformations III. Face-centred cubic to body-centred tetragonal transformations, Acta Metallurgica. 2 (1954) 224–234. https://doi.org/10.1016/0001-6160(54)90163-7.

[48] J.K. Mackenzie, J.S. Bowles, The crystallography of martensite transformations II, Acta Metallurgica. 2 (1954) 138–147. https://doi.org/10.1016/0001-6160(54)90103-0.

Declaration of interests

☒The authors declare that they have no known competing financial interests or personal relationships that could have appeared to influence the work reported in this paper.

☐The authors declare the following financial interests/personal relationships which may be considered as potential competing interests: